Check for updates

One-pot synthesis of cubic PtPdCu nanocages with enhanced electrocatalytic activity for reduction of H₂O₂

Liangliang Tian, [iD] *[ab] Yanling Chen,[ab] Shenping Wu,[ab] Yanhua Cai,[ab] Hongdong Liu,[ab] Jin Zhang,[ab] Cong Yang,[ab] Gege He,[ab] Wei Xiao, [iD] *[ab] Lu Li,[ab] Li Lin[ab] and Yue Cheng[ab]

Despite the high electrocatalytic activity of Pt, pure Pt electrocatalysts always suffer from high cost and poor poison resistance. In this work, a cubic PtPdCu nanocage (NC) trimetallic electrocatalyst was synthesized using cuprous oxide as a sacrificial template. Being employed as a H_2O_2 detection electrode, PtPdCu NCs exhibit higher sensitivity (562.83 μA mM^{-1} cm^{-2}) than that of PdCu NCs (210.19 μA mM^{-1} cm^{-2}), PtCu NCs (411.34 μA mM^{-1} cm^{-2}) and commercial Pt black (16.94 μA mM^{-1} cm^{-2}). Furthermore, a PtPdCu NCs electrode presents a working potential as low as 0.05 V. The excellent electrocatalytic activity can be attributed to the suitable hollow porous structure and synergistic electrocatalysis effect between Pt, Pd and Cu. It is believed that the trimetallic PtPdCu NCs electrocatalyst has potential applications in the design of H_2O_2 detection electrodes.

1. Introduction

Nowadays, it is still of great importance to develop H_2O_2 sensors due to their crucial applications in clinical medicine, biochemistry, pharmaceuticals, food safety and environmental monitoring.[1,2] As a classical electrocatalyst, Pt nanoparticles can significantly decrease the overpotential of H_2O_2 during electrocatalytic processes.[3,4] However, the rare reserves, high cost and poor poison resistance of single Pt dramatically limit its practical applications.

Design of Pt-based bi- or trimetallic nanostructures is an effective route to reduce the consumption of Pt and improve its activity for multistep catalysis.[5,6] Recent reports indicate that Pd alloying can promote the poison resistance and electrocatalytic activity of Pt.[7,8] In the case of H_2O_2, Pd atoms close to Pt could take OH_{ad} on Pd sites and highly active Pt mainly functions as actives for H_2O_2, leading to a bifunctional electrocatalytic mechanism.[9] On the other hand, alloying of noble metals with transition metals (Fe, Co, Ni, Sn, Cu, *etc.*) is another approach to enhance the electrocatalytic performance. Transition metals alloying not only saves noble metals but also causes a negative shift of d-band center position and rearrangement of the surface atoms, resulting in easy desorption of intermediate products and a high active surface.[10] Thus, synthesis of transition metal alloyed PtPd is an efficient way to design high-efficiency electrocatalyst for H_2O_2.

In this paper, Cu alloyed cubic PtPd NCs were synthesized using Cu_2O as sacrificial templates and employed to construct amperometric H_2O_2 sensor. The hollow porous architecture provides large surface area and abundant diffusion paths for analyte and electrolyte, which is benefit for electrocatalytic kinetics. As a detection electrode for H_2O_2, the PtPdCu NCs electrode presents excellent electrocatalytic activity in terms of high sensitivity and eminent anti-poisoning performance due to the synergistic electrocatalysis effect.

2. Materials and methods

2.1 Synthesis of cubic PtPdCu NCs

Cubic Cu_2O was synthesized according to the previous report.[11] 10.0 mL NaOH solution (2 M) was dropped into the stirred $CuCl_2 \cdot 2H_2O$ (100 mL, 0.01 M) at 55 °C. 10.0 mL ascorbic acid (0.6 M) was added after 30 min. The brick-red products were centrifuged after 3 h, followed by drying in vacuum at 40 °C overnight.

For the preparation of PtPdCu NCs, 10 mg as-prepared Cu_2O was dispersed into 10 mL distilled water by ultrasonic for 15 min. Then a mixed solution containing 1 mL chloroplatinic acid (20 mM) and 0.6 mL disodium tetrachloropalladate (33 mM) was added (the mole ratio of Pt and Pd is 1 : 1). After reacting for 30 min, 1 mL $NH_3 \cdot H_2O$ (1 : 1) was injected to etch the residual Cu_2O cores. The ultimate products were separated by mild centrifugation after 12 h and dried at 40 °C for 24 h. PtCu NCs and PdCu NCs samples were also synthesized under the same condition using chloroplatinic acid or disodium tetrachloropalladate only.

[a]Research Institute for New Materials Technology, Chongqing University of Arts and Sciences, Chongqing, PR China. E-mail: tianll07@163.com; showame@aliyun.com
[b]Co-innovation Center for Micro/Nano Optoelectronic Materials and Devices, PR China

2.2 Electrochemical measurements

All electrochemical measurements were performed in 0.1 M phosphate buffer solution (PBS, pH = 7.0). A three-electrode configuration was applied with Ag/AgCl (saturated with KCl) and platinum disk as the reference and counter electrode, respectively. PtPdCu NCs, PtCu NCs, PdCu NCs and Pt black modified glassy carbon electrodes (GCE, Φ = 3 mm) were employed as the working electrodes. Typically, GCE was polished with 3 μm, 0.5 μm and 0.05 μm alumina powders, respectively. Then, 5 μL of suspension (1 mg mL^{-1} in 0.1 wt% Nafion solution) was cast onto the polished GCE and finally dried by infrared.

2.3 Materials characterizations

The phase and structure of PtPdCu NCs were characterized by X-ray diffraction (XRD) performed on a Rigaku D/Max-2400 X-ray diffractometer using Cu Kα radiation (40 kV, 60 mA). The chemical state was determined by X-ray photoelectron spectroscopy ESCALAB 250Xi (XPS, USA) using 500 μm X-ray spot and all the XPS spectra were calibrated by C 1s line at 284.8 eV. The morphologies and microstructures of PtPdCu NCs were analyzed on Hitachi S-4800 field emission scanning electron microscope (FESEM) and FEI F20 high-resolution transmission electron microscope (HRTEM). Specific surface area and porosity measurements were conducted on a Belsort-max instrument using N$_2$ adsorption–desorption isotherms.

3. Results and discussions

3.1 Characterizations

The surface state and composition of the products were confirmed by XPS. As shown in Fig. 1a, Pt 4f and Cu 3p are overlapped between 65.5 eV and 83.5 eV. The peaks located at 70.8 eV and 73.9 eV correspond to Pt 4f$_{7/2}$ and Pt 4f$_{5/2}$, and the peaks at 75.2 eV and 77.3 eV can be related to Cu 3p$_{3/2}$ and Cu 3p$_{1/2}$, respectively, demonstrating the coexist of Pt and Cu in the products. The observed peaks at 335.1 eV and 340.5 eV in Fig. 1b correspond to 3d$_{5/2}$ and 3d$_{3/2}$ of Pd, respectively.[12] In Fig. 1c, the peaks located at binding energy of 932.4 eV and 952.3 eV refer to Cu 2p$_{3/2}$ and Cu 2p$_{1/2}$, respectively, which is well consistent with pure Cu. According to XPS results, the atomic ratio of Pt, Pd and Cu is 37 : 42 : 21. Although the same amounts of PtCl$_6^{2-}$ and Pd^{2+} were added, the atom content of Pd is slightly higher than Pt. The reactivity between Pd^{2+} and Cu$_2$O is much higher than that between PtCl$_6^{2-}$ and Cu$_2$O. Hence, a Pd-rich layer would preferentially form around Cu$_2$O and hinder the diffusion of fresh reagent, resulting in higher Pd content in the products. In XRD pattern (Fig. 1d), all the reflection peaks can be indexed to (111), (200), and (220) diffractions of face-centered-cubic structure. No refection peaks of Cu$_2$O are observed in all the XRD patterns, confirming the purity of products. The reflection peaks of PtPdCu display a slight positive shift compared to PtCu, however, a negative shift compared to PdCu, indicating the successful preparation of PtPdCu alloys.[13] The analysis of XPS and XRD confirm the successful preparation of PtPdCu NCs.

The difference between electrode potentials is considered to be the driving force for the reactions. The redox pair value of Cu$_2$O/Cu (0.36 V) is much lower than that of PtCl$_6^{2-}$/Pt (0.735 V) and Pd/Pd^{2+} (0.987 V). Thus, Cu$_2$O crystals can be employed as reducing agent for PtCl$_6^{2-}$ and Pd^{2+}. The formation mechanism of Pt and Pd can be explained as follows:[13]

$$2Cu_2O + 4H^+ + PtCl_6^{2-} \rightarrow Pt + 4Cu^{2+} + 6Cl^- + 2H_2O \quad (1)$$

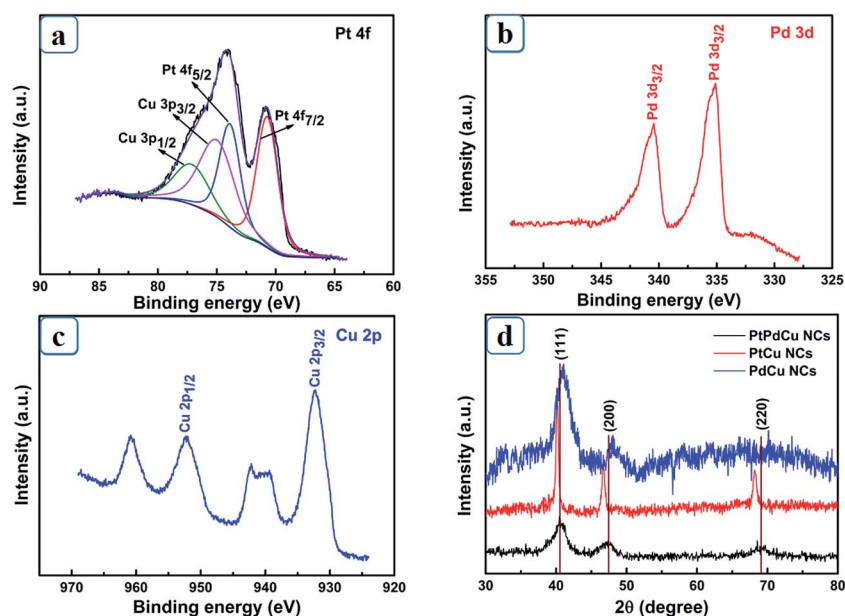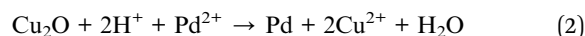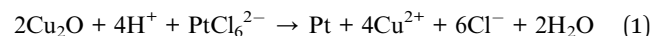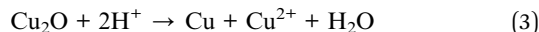$$Cu_2O + 2H^+ + Pd^{2+} \rightarrow Pd + 2Cu^{2+} + H_2O \quad (2)$$

Fig. 1 XPS spectra for the products. (a) Pt 4f; (b) Pd 3d; (c) Cu 2p; (d) XRD patterns of prepared PtPdCu, PtCu and PdCu.

Cu atoms in the products can be ascribed to the disproportionation of Cu(I) in the presence of H$^+$:

$$Cu_2O + 2H^+ \rightarrow Cu + Cu^{2+} + H_2O \qquad (3)$$

Above reactions can simultaneously produce Pt, Pd and Cu atoms, resulting in the formation of PtPdCu alloys around Cu$_2$O templates. Finally, Cu$_2$O cores were removed by etching and PtPdCu NCs were successfully constructed.

Morphologies of the products were observed by SEM and TEM and the images were displayed in Fig. 2. As shown in Fig. 2a, the prepared Cu$_2$O presents smooth cubic characteristics with an edge length about 500 nm. After reaction, cubic feature of Cu$_2$O is exactly replicated by PtPdCu alloy (Fig. 2b) and the surface turns into rough and porous. The partly broken cube in Fig. 2b reveals the hollow cage-like structure of PtPdCu. The porous architecture affords amounts of paths for diffusion of analyte and desorption of intermediate products, which favours the electrocatalytic kinetics. Further insight into the details, PtPdCu NCs are constructed by aggregations of fine PtPdCu nanograins (Fig. 2c). TEM image of PtPdCu NCs in Fig. 2d provides convincing evidence for the cubic hollow structure of PtPdCu. A well-defined cubic PtPdCu NC was investigated in Fig. 2e and the shell of the cube is around 80 nm. As depicted in Fig. 2f, the grain size of PtPdCu NCs is about 4 nm. The spacing for marked adjacent lattice fringes is about 0.2218 nm, which is smaller than that of pure Pt (111) (0.2245 nm) and Pd (111) (0.2265 nm) but larger than pure Cu (111) (0.2088 nm), implying the formation of ternary PtPdCu alloy.

For the characterizations of specific surface area and porosity, N$_2$ adsorption–desorption isotherms and Barrett–Joyner–Halenda pore size distributions were measured. As shown in Fig. 3a, PtPdCu NCs possess a large specific surface area of 98.8 m^2 g^{-1}, which is much larger than that of PtCu NCs (61.9 m^2 g^{-1}) (Fig. 3b) and PdCu NCs (58.7 m^2 g^{-1}) (Fig. 3c). In addition, a larger pore volume of 0.16 cm^3 g^{-1} is observed for PtPdCu NCs compared to PtCu NCs (0.092 cm^3 g^{-1}) and PdCu NCs (0.088 cm^3 g^{-1}). PtPdCu NCs, PtCu NCs and PdCu NCs present similar pore size distributions with mean pore diameters of 5.2 nm, 5.7 nm and 6.3 nm, respectively. On the basis of above discussions, PtPdCu NCs could offer more contact area and diffusion channels for electrolyte, which is beneficial for electrocatalysis.

3.2 Electrochemical performance

PtPdCu NCs were employed to detect H$_2$O$_2$ to evaluate its electrocatalytic activity. Fig. 4a displays the cyclic voltammetry curves (CVs) of different electrodes, largest current response is observed for PtPdCu NCs electrode at 0.05 V compared to PtCu NCs and PdCu NCs, demonstrating higher electrocatalytic activity towards electroreduction of H$_2$O$_2$. As can be seen from Fig. 4b, the peak current at 0.05 V linearly scales with the increase of H$_2$O$_2$ concentration, confirming potential applications for detect H$_2$O$_2$. CVs of PtPdCu NCs with different scan rates were recorded in Fig. 4c to estimate its kinetics process. Both the anodic peak current (peak 2 and 3) and cathodic peak current (peak 1) are proportional to the square root of scan rates (Fig. 4d), indicating a typical diffusion-controlled electrocatalytic process.[14]

Typical amperometric responses of PtCu, PdCu, PtPdCu NCs and commercial Pt black electrodes at 0.05 V were recorded in Fig. 5a. PtCu NCs electrode presents higher current response than commercial Pt. The improved electrocatalytic activity is related to the hollow porous feature and the alloying of Cu atoms. The introduced Cu atoms not only result in a high-active Pt-rich surface in the outermost layer but also reduce the Pt–OH$_{ad}$ bonding strength, accelerating the regeneration of Pt actives.[8,10] Moreover, the PtCu NCs electrode displays broader linear range than commercial Pt, implying better anti-poisoning performance towards intermediate products. Obviously, PtCu NCs electrode shows higher current response than PdCu NCs
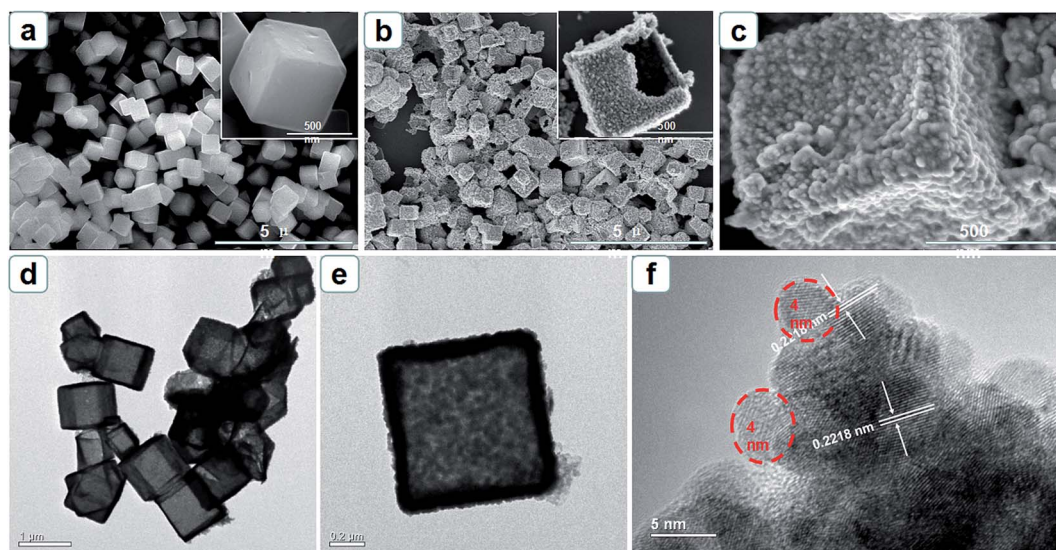

Fig. 2 SEM images of (a) cubic Cu$_2$O and (b, c) PtPdCu NCs; (d, e) TEM and (f) HRTEM images of PtPdCu NCs.
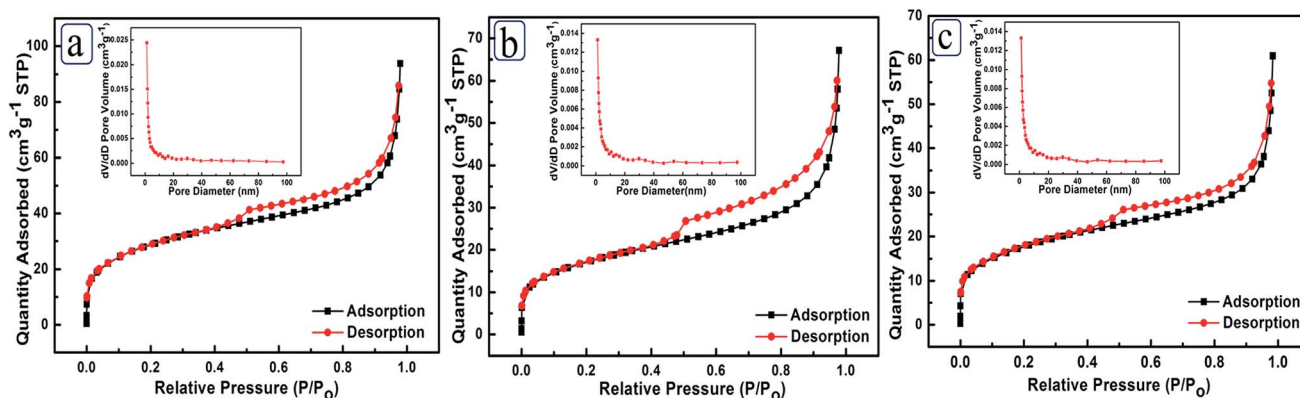
Fig. 3 N$_2$ adsorption–desorption isotherms of (a) PtPdCu NCs, (b) PtCu NCs and (c) PdCu NCs. Insets are the corresponding pore size distributions, respectively.

electrode, indicating that Pt sites are the main electroreduction active sites for H$_2$O$_2$. The alloyed Pd atoms modulates the surface electronic structure of PtCu NCs and acts as promoting centers for the generation of OH$_{ad}$ species, guaranteeing the activity of Pt active.[15] PtPdCu NCs electrode displays larger response current compared to PtCu NCs, PdCu NCs and commercial Pt black electrodes, confirming the advantages of designed microstructure and synergistic electrocatalytic effect.[16] From Fig. 5b, the response current of PtPdCu NCs electrode linearly increases with the H$_2$O$_2$ concentration between 1.5 μM (limit of detection) and 11.6 mM with a sensitivity of 562.83 μA mM^{-1} cm^{-2}, which is higher than that of

PdCu NCs (210.19 μA mM^{-1} cm^{-2}), PtCu NCs (411.34 μA mM^{-1} cm^{-2}) and commercial Pt black (16.94 μA mM^{-1} cm^{-2}). The sensing performance of PtPdCu NCs electrode was compared with other reported Pt-based electrodes in Table 1. It is found that PtPdCu NCs electrode presents low overpotential, high sensitivity and wide linear range towards detection of H$_2$O$_2$. The excellent electrocatalytic activity can be essentially attributed to large surface area and highly porous architecture of PtPdCu NCs electrode, which is benefit for diffusion of analyte and desorption of intermediate products.

Selectivity of PtPdCu NCs electrode was estimated by adding one-tenth ascorbic acid (AA), uric acid (UA), lactose (Lact.),
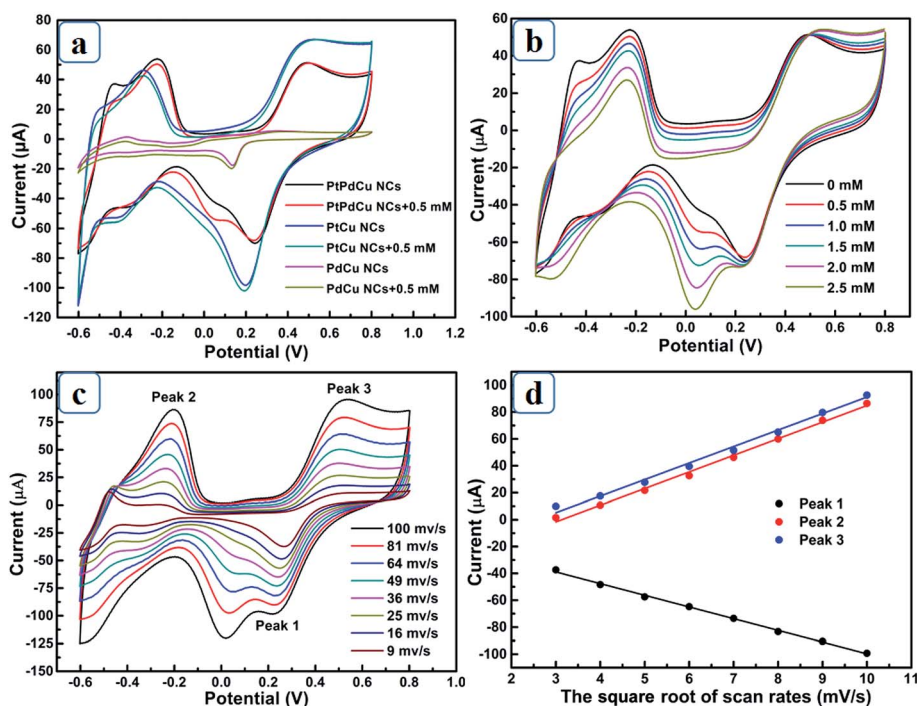

Fig. 4 (a) CVs of PtCu NCs, PdCu NCs and PtPdCu NCs electrodes with and without H$_2$O$_2$ in neutral PBS solution; (b) CVs of PtPdCu NCs electrode with different concentration of H$_2$O$_2$; (c) CVs of PtPdCu NCs electrode at various scan rates in neutral PBS solution with 0.5 mM H$_2$O$_2$; (d) the relationship between peak current and square root of scan rates.
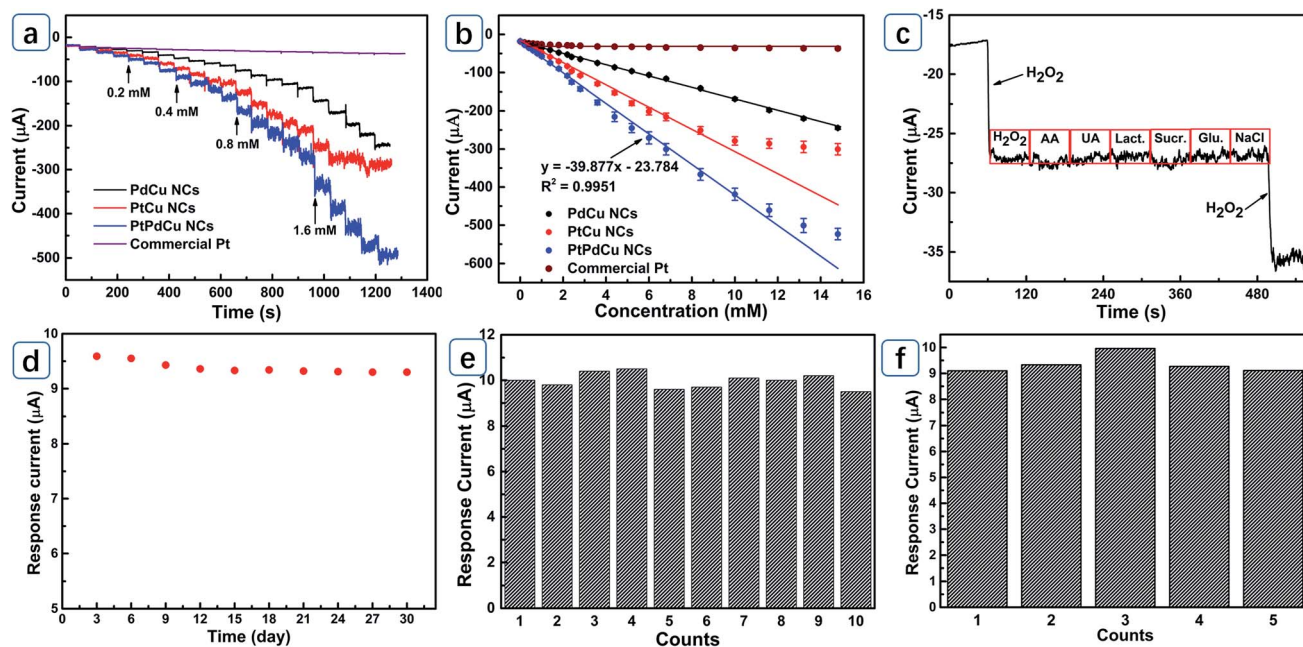
Fig. 5 (a) Amperometric responses of PtCu NCs, PdCu NCs, PtPdCu NCs and commercial Pt black electrodes at 0.05 V with the successive addition of H_2O_2; (b) the relationship between response current and the injected concentration of H_2O_2 for different electrodes; (c) current responses of PtPdCu NCs electrode towards sequential injection of 0.02 mM interfering species after initial injection of 0.2 mM H_2O_2 at an applied potential of 0.05 V; (d) long term stability of PtPdCu NCs electrode; (e) ten measurements of a PtPdCu electrode towards 0.2 mM H_2O_2; (f) current responses of five prepared electrodes towards 0.2 mM H_2O_2.

sucrose (Sucr.), glucose (Glu.) and NaCl species during H_2O_2 detection at 0.05 V (Fig. 5c). PtPdCu NCs electrode only present mild interference towards AA (4.5%) and sucrose (5.4%). In addition, the second addition of 0.2 mM H_2O_2 retains about 93% of its original response, demonstrating excellent selectivity and anti-poisoning performance. Long term stability of the PtPdCu NCs electrode was tested by recording the current responses for 0.2 mM H_2O_2 for 30 days (Fig. 5d). PtPdCu NCs electrode still retains 97% of its original current response, revealing excellent stability. The reproducibility of PtPdCu NCs electrode was tested by measuring its response current towards 0.2 mM H_2O_2 for ten times and the relative standard deviation (RSD) for current response is about 3.34% (Fig. 5e). In addition,

the current responses towards 0.2 mM H_2O_2 of five different electrodes were recorded and the RSD for current responses is about 3.63% (Fig. 5f). PtPdCu NCs electrode possesses low applied potential, high sensitivity, reliable stability and excellent reproducibility, indicating potential practicability in nonenzymatic H_2O_2 electrochemical sensor.

4.   Conclusions

In conclusions, cubic PtPdCu NCs synthesized by sacrificial template method were applied to detect H_2O_2. The electrode exhibits excellent electrocatalytic activity towards H_2O_2 in terms of low applied potential, high sensitivity, reliable stability and

Table 1 Comparison of researched electrode with reported nonenzymatic H_2O_2 sensors based on Pt

Electrode	Potential (V)	Sensitivity ($\mu A\ mM^{-1}\ cm^{-2}$)	Linear range (mM)	Reference
PtPdCu NCs	0.05 (Ag/AgCl)	562.8	0.0015–11.6	This work
3,4-Ethylenedioxythiophene-Pt NPs[a]	−0.55 (Ag/AgCl)	19.3	0.0016–6	17
Pt–MnO$_x$	0.35(Ag/AgCl)	123	0.002–4	18
Pt–SnO$_2$@C	0.5 (—)	241	0.001–0.17	19
MWCNTs/Pt NHs[b]	0 (Ag/AgCl)	205.8	0.01–2	20
Pt/PPy/GCE[c]	−0.1 ((Ag/AgCl))	80.4	1–8	21
Pt$_{0.5}$Au$_{0.5}$@C	0.3 (Ag/AgCl)	210.3	0.007–6.5	22
Nafion/Pt NPs[a]/RGO[d]	−0.1 (Ag/AgCl)	132.8	0.005–3	23
Pt flowers/gold slice	−0.2 (Ag/AgCl)	314	0.1–0.9	24
PDDA[e]/Pt	0.6 (Ag/AgCl)	500	0.000042–0.16	25

[a] Nanoparticles. [b] MWCNTs = multi-wall carbon nanotubes; NDs = nanohybrids. [c] PPy = polypyrrole; GCE = glassy carbon electrode. [d] Reduced graphene oxide. [e] Poly(diallydimethylammonium chloride).

excellent reproductivity. It is believed that the hollow porous PtPdCu NCs have potential applications in design of electrochemical sensors.

Acknowledgements

References

1 W. Lian, L. Wang, Y. Song, H. Yuan, S. Zhao, P. Li and L. Chen, *Electrochim. Acta*, 2009, **54**, 4334–4339.
2 M. Q. Wang, Y. Zhang and S. J. Bao, *Electrochim. Acta*, 2016, **190**, 365–370.
3 K. Huang, Y. Li and Y. Xing, *Electrochim. Acta*, 2013, **103**, 44–49.
4 L. L. Tian, X. H. Zhong, W. P. Hu, B. T. Liu and Y. Li, *Nanoscale Res. Lett.*, 2014, **9**, 68–72.
5 D. S. Wang and Y. D. Li, *Adv. Mater.*, 2011, **23**, 1044–1060.
6 B. Y. Xia, H. B. Wu, X. Wang and X. W. Lou, *J. Am. Chem. Soc.*, 2012, **134**, 13934–13937.
7 X. Q. Huang, Y. J. Li, Y. J. Li, H. L. Zhou, X. F. Duan and Y. Huang, *Nano Lett.*, 2012, **12**, 4265–4270.
8 X. H. Niu, C. Chen, H. L. Zhao, Y. Chai and M. B. Lan, *Biosens. Bioelectron.*, 2012, **36**, 262–266.
9 Y. B. Zhou, G. Yu, F. F. Chang, B. N. Hu and C. J. Zhong, *Anal. Chim. Acta*, 2012, **757**, 56–62.
10 V. R. Stamenkovic, B. Fowler, B. S. Mun, G. F. Wang, P. N. Ross, C. A. Lucas and N. M. Markovic, *Science*, 2007, **315**, 493–497.
11 D. F. Zhang, H. Zhang, L. Guo, K. Zheng, X. D. Han and Z. Zhang, *J. Mater. Chem.*, 2009, **19**, 5220–5225.
12 H. M. Duan and C. X. Xu, *Electrochim. Acta*, 2015, **152**, 417–424.
13 F. Hong, S. D. Sun, H. J. You, S. C. Yang, J. X. Fang, S. W. Guo, Z. M. Yang, B. J. Ding and X. P. Song, *Cryst. Growth Des.*, 2011, **11**, 3694–3697.
14 M. R. Guascito, E. Filippo, C. Malitesta, D. Manno, A. Serra and A. Turco, *Biosens. Bioelectron.*, 2008, **24**, 1057–1063.
15 A. X. Yin, X. Q. Min, W. Zhu, W. C. Liu, Y. W. Zhang and C. H. Yan, *Chem.–Eur. J.*, 2012, **18**, 777–782.
16 J. Lan, K. Wang, Q. Yuan and X. Wang, *Mater. Chem. Front.*, 2017, **1**, 1217–1222.
17 L. C. Chang, H. N. Wu, C. Y. Lin, Y. H. Lai, C. W. Hu and K. C. Ho, *Nanoscale Res. Lett.*, 2012, **7**, 319–326.
18 H. Kivrak, O. Alal and D. Atbas, *Electrochim. Acta*, 2015, **176**, 497–503.
19 H. Lu, S. Yu and F. Yang, *Colloids Surf., B*, 2012, **101**, 106–110.
20 Z. Miao, D. Zhang and Q. Chen, *Materials*, 2014, **7**, 2945–2955.
21 X. J. Bian, X. F. Lu, E. Jin, L. R. Kong, W. J. Zhang and C. Wang, *Talanta*, 2010, **81**, 813–818.
22 O. G. Sahin, *Electrochim. Acta*, 2015, **180**, 873–878.
23 C. Zhang, H. Jiang, R. Ma, Y. Y. Zhang and Q. Chen, *Ionics*, 2017, 1–9, DOI: 10.1007/s11581-016-1944-2.
24 J. Wan, W. Wang and G. Yin, *J. Cluster Sci.*, 2012, **23**, 1061–1068.
25 P. Karam and L. I. Halaoui, *Anal. Chem.*, 2008, **80**, 5441–5448.